

Deciphering a Reaction Network for the Switchable Production of Tetrahydroquinoline or Quinoline with MOF-Supported Pd Tandem Catalysts

Long Qi,^{*,||} Jingwen Chen,^{||} Biying Zhang, Renfeng Nie, Zhiyuan Qi, Takeshi Kobayashi, Zongbi Bao, Qiwei Yang, Qilong Ren, Qi Sun, Zhiguo Zhang,^{*} and Wenyu Huang^{*}



Cite This: <https://dx.doi.org/10.1021/acscatal.0c00899>



Read Online

ACCESS |

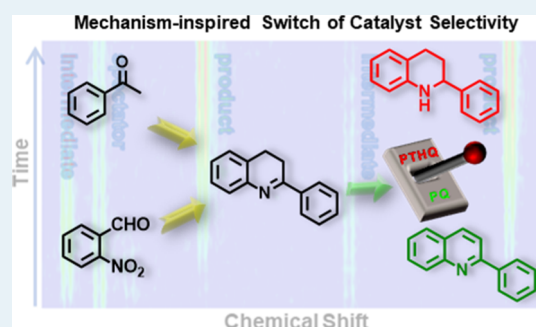
Metrics & More

Article Recommendations

Supporting Information

ABSTRACT: A mechanistic study of heterogeneous tandem catalytic systems is crucial for understanding and improving catalyst activity and selectivity but remains challenging. Here, we demonstrate that a thorough mechanistic study of a multistep reaction can guide us to the controllable selective synthesis of phenyltetrahydroquinoline or phenylquinoline with easily accessible precursors. The one-pot production can be achieved, catalyzed by a well-defined, bifunctional metal–organic framework-supported Pd nanoparticles, with only water as the side product. Our mechanistic study identifies six transient intermediates and ten transformation steps from the operando magic angle spinning nuclear magnetic resonance study under 27.6 bar H₂. In particular, reactive intermediate 2-phenyl-3,4-dihydroquinoline cannot be observed with conventional chromatographic techniques but is found to reach the maximal concentration of 0.11 mol L⁻¹ under the operando condition. The most probable reaction network is further deduced based on the kinetic information of reaction species, obtained from both operando and *ex situ* reaction studies. This deep understanding of the complex reaction network enables the kinetic control of the conversions of key intermediate, 2-phenyl-3,4-dihydroquinoline, with the addition of a homogeneous co-catalyst, allowing the selective production of tetrahydroquinoline or quinoline on demand. The demonstrated methods in this work open up new avenues toward efficient modulation of reactions with a complex network to achieve desired selectivities.

KEYWORDS: tandem catalysis, reaction network, metal–organic frameworks, metal nanoparticles, operando spectroscopy, mechanistic study



INTRODUCTION

The concept of tandem catalysis, whereby sequential chemical conversions catalyzed by multiple active sites in one pot giving the desirable product selectively, has gained significant interest for the selective catalytic production of chemicals and fuels.¹ This interest is based on the prospects of boosting the atom economy, as costly intermediate separations and purification processes could be avoided. Identified among the five priority research directions for catalysis science by U.S. DOE in 2017,² a significant challenge is how to direct convoluted transformations through the desired routes for the target product in a complexed reaction network, given that tandem catalysis typically involves multiple transiently evolved intermediates. Thus far, optimization of reaction conditions has relied mainly on laborious and time-consuming trial-and-error experiments. The establishment of complex reaction networks, including reactants, intermediates, and favored and unwanted products, would help to elucidate the underlying principles of such transformations and, in turn, guide the design of efficient catalytic systems.

Probing the reaction network requires but is not limited to: (1) identifying reaction species, (2) deconvoluting individual reaction paths, and (3) understanding the reversibility and rates of interconversions. However, because of the co-presence of solid catalysts, reaction solution, and reactive gas, an in-depth study of heterogeneous tandem reactions and the associated complexed reaction network is rather challenging, in particular when intermediates are unstable upon sampling. Even for stable species, the limited number of intermittent sampling at high temperature and pressure greatly restricts the data density to delineate the reaction network accurately.

Advanced techniques as noteworthy as operando magic angle spinning nuclear magnetic resonance (NMR) spectroscopy

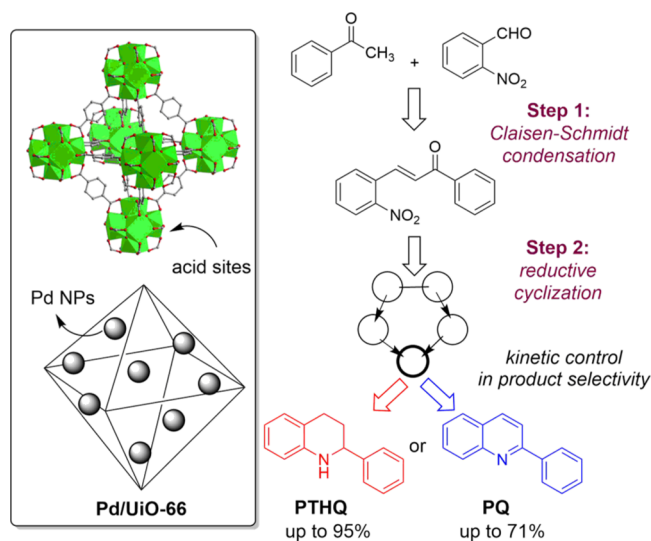
Received: February 23, 2020

Revised: March 15, 2020

Published: March 17, 2020

copy (MAS-NMR)³ has proven to be unique for detailed structural and kinetic information of multiphase systems at both high temperatures and high pressures.^{4,5} Accordingly, operando MAS-NMR techniques provide the opportunity for monitoring the reaction intermediates and ultimately mapping out the reaction networks. To elaborate the feasibility of our plan, we choose a model tandem catalytic system for the production of tetrahydroquinoline (THQ) or quinoline, where the first chemical conversion is the Claisen–Schmidt condensation of 2-nitrobenzaldehyde (NBA) and acetophenone (ACP) to nitrochalcone, followed by its reductive intramolecular cyclization (Scheme 1). This reaction is ideal

Scheme 1. Kinetic Control in the Selective Synthesis of PTHQ and PQ Catalyzed by Pd/Uio-66



not only because the production of THQ and quinoline architectures, widely existing in bioactive natural products,⁶ can serve as key pharmaceutical ingredients,^{7–13} and THQ is essential building block of hydrogen-storage materials,^{14–16} but also because of the involvement of multiple transiently evolved intermediates as a result of the concurrent reduction of several functionalities (i.e., $-\text{NO}_2$, $\text{C}=\text{C}$, $\text{C}=\text{O}$, $\text{C}=\text{N}$, and arenes) during reductive cyclization.

In order to thoroughly study this tandem reaction and gain insights into the fundamental principles behind, a stable, well-defined catalyst is necessary. Metal–organic frameworks (MOFs) give great promises for the integration of multiple active species for tandem catalysis. By judiciously selecting the metal centers/clusters and ligands of the MOF, a micro-environment is created, which can be used to introduce other catalytic species further and aid the catalytic process. Considering that active species with acidity and hydrogenation capability are needed to accomplish the aforementioned transformations, we constructed a bifunctional catalyst by supporting Pd nanoparticles (NPs) on an acidic MOF, that is, Pd/Uio-66 (Scheme 1). Using the advanced operando spectroscopic method, we detected and quantified key intermediates (under 27.6 bar H_2 at 40 °C), in particular, the reactive 2-phenyl-3,4-dihydroquinoline and (*E*)-3-(2-(hydroxyamino)phenyl)-1-phenylprop-2-en-1-one that cannot be detected by *ex situ* sampling methods. Significantly, the obtained mechanistic information was then utilized to unravel the high selectivity in the phenylTHQ (PTHQ) synthesis for

the Pd/Uio-66 catalyst. More importantly, the mechanistic insights further allowed us to switch the selectivity of the product between PTHQ and phenylquinoline (PQ) by adding a co-catalyst. These results provide a new insight for manipulating complex transformations.

RESULTS AND DISCUSSION

Production of PTHQ with Bifunctional Pd/Uio-66.

MOFs have attracted great attention as solid acid catalysts.^{17–20} Modifying the organic linkers or immobilizing metal NPs also introduces other active sites.^{21–23} The co-existence of different active sites can enable tandem catalysis of two or more consecutive steps in one pot to eliminate unnecessary separation/purification steps and boost the atom economy.^{1,24}

In the multistep synthesis of PTHQ (Scheme 1), we first carried out the Claisen–Schmidt condensation between ACP (1) and NBA (2) at 100 °C with three different acidic MOFs, including Uio-66(Zr), HKUST(Cu), and MIL-101(Cr). The structural characterization results of these three MOFs are shown in Figures S1 and S2. Uio-66 shows the highest catalytic activities achieving the quantitative yield of *ortho*-nitrochalcone (4) in 3 h (Figure 1). The high activity could be

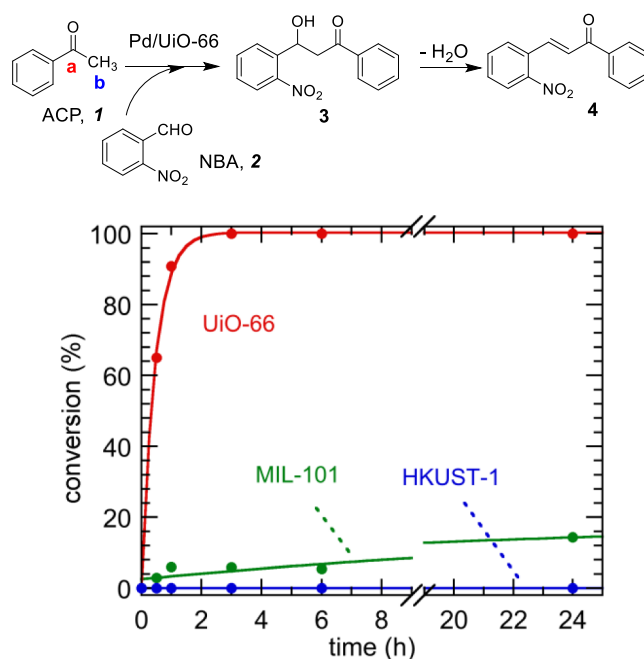


Figure 1. Conversion of NBA versus reaction time for the MOF-catalyzed Claisen–Schmidt condensation reaction. Reaction conditions: NBA (0.2 mmol), ACP (0.4 mmol), catalyst (5 mg), toluene (1 mL), and 100 °C. Lines are added only to guide the eye.

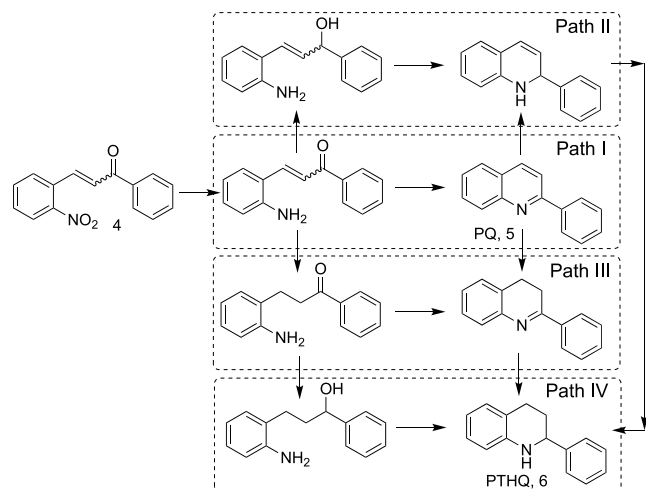
owing to the combined efforts of Lewis acidic Zr with the missing ligand and Brønsted site by the μ_3 -OH in the SBU.^{25,26} The strong Lewis acidity has been demonstrated in the Meerwein–Ponndorf–Verley reduction of prenol and furfural.²⁷ MIL-101 with coordination-unsaturated Cr sites show only 8% conversion in 3 h, which is much less active when compared to Uio-66. Lewis acidic HKUST-1 is inefficient in promoting the condensation reaction, although it is active in catalyzing the Friedländer reaction for the synthesis of quinoline.²⁸ In comparison, an inorganic solid acid, γ - Al_2O_3 , was examined and found nearly inactive as well. Therefore,

131 UiO-66 is chosen as the acidic catalyst for the multistep
132 reaction.

133 To introduce hydrogenation capability to the MOF, we
134 synthesized Pd NPs supported on UiO-66 via wetness
135 impregnation followed by reduction under flowing H₂.²⁹ The
136 powder X-ray diffraction patterns show that UiO-66 and Pd/
137 UiO-66 match the simulated pattern of the MOF (Figure
138 S1A), indicating that the MOF structure is maintained after the
139 loading of Pd NPs (2 wt %). The Brunauer–Emmett–Teller
140 (BET) surface areas of UiO-66 before and after loading Pd are
141 1800 and 1530 m²·g⁻¹, respectively (Figure S1C and Table
142 S1). The micropore volume of UiO-66 also decreases slightly
143 from 0.50 to 0.46 cm³·g⁻¹. X-ray diffraction peaks of Pd NPs
144 were not obvious, possibly because of the low metal loading.
145 As shown in the transmission electron microscopy images
146 (Figure S1B), the Pd NPs are dispersed uniformly mostly on
147 the external surface of UiO-66 with an average diameter of 4.2
148 ± 0.7 nm. Kinetic studies revealed that the catalytic activity of
149 UiO-66 in the Claisen–Schmidt condensation reaction only
150 slightly decreased after loading Pd NPs.

151 The production of PQ or PTHQ can be achieved via
152 cyclization after reduction of –NO₂ in **4**. The cyclization can
153 proceed in four possible paths (Scheme 2): (I) condensation

Scheme 2. Reductive Cyclization of **4** to PTHQ Catalyzed by Pd/UiO-66, Showing Four Possible Cyclization Paths^a



^aPossible reactant H₂ and product H₂O are omitted.

154 of –NH₂ and C=O to form PQ as the direct key
155 intermediate; (II) condensation of –NH₂ and –OH via
156 nuclear substitution to form intermediate 2-phenyl-1,2-
157 dihydroquinoline after reduction of C=O; (III) condensation
158 of –NH₂ and C=O to form intermediate 2-phenyl-1,2-
159 dihydroquinoline after reduction of C=C; and (IV)
160 condensation of –NH₂ and –OH via nuclear substitution to
161 form PTHQ directly after reduction of both C=C and C=O.

162 Before carrying out the one-pot tandem synthesis of PTHQ
163 from NBA and ACP (discussed in a latter section), we
164 conducted reductive cyclization (Step 2) of **4** which was
165 isolated from the condensation reaction mixture (Step 1).
166 Their concentration profiles follow pseudo first-order rate law
167 when the hydrogen gas is in large excess, and the catalyst
168 concentration remains unchanged; therefore, the results are
169 presented as normalized concentrations, as shown in Figure
170 2.³⁰ The conversion of **4** was completed in 5 h with the 56%

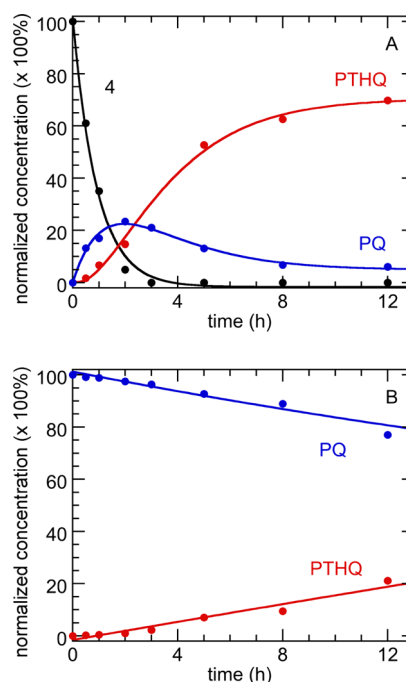


Figure 2. Time-resolved concentration profiles of the Pd/UiO-66-catalyzed hydrogenation reaction of (A) **4** and (B) PQ at 40 °C and 27.6 bar H₂. Reaction conditions: substrate (0.2 mmol), 2 wt % Pd/UiO-66 (5 mg, ~0.5 mmol % Pd), and solvent toluene (2 mL). Conversions were calculated based on analysis of GC results. Lines are added to guide the eye.

yield to PTHQ at 40 °C under 27.6 bar H₂ (Figure 2A). PQ is
also formed from **4** (Figure 2A), reaching maximal yields of
23% at 2 h. To determine whether the hydrogenation of PQ is
the major reaction path to PTHQ, we tested the hydro-
genation of PQ under the same conditions. The PTHQ
production from PQ was significantly slower than that from **4**
(Figure 2B). These results suggest that PQ is a side product
rather than the rate-limiting intermediate toward PTHQ,
which is also confirmed by the hydrogenation of **4** and PQ
under ambient-pressure H₂ at 50 °C (Figure S3). Furthermore,
there is a mass loss with **4** as the reactant, which cannot be
accounted for with any peaks in gas chromatograms.

Mechanistic Study with Operando MAS-NMR. To
further maximize production of PQ or PTHQ, it is crucial to
understand the reaction network leading to their formation,
which is not obviously based on *ex situ* studies. Previous
studies by Crabtree³¹ and Soós³² used spectroscopic and
density functional theory methods for the simple reduction of
quinolines to THQs using homogeneous catalysts. Similar
approaches cannot be readily applied to heterogeneous
catalytic systems because of the complexity of the molecular
transformation in our multiphasic reaction systems. Therefore,
we employed operando high-pressure MAS-NMR studies to
explore the reaction network.

The high-pressure MAS rotor^{33,34} was loaded with ACP,
NBA (0.83 equiv), and Pd/UiO-66 in toluene. The ACP was
isotopically labeled at both *a*- and *b*-positions with ¹³C (194.5
and 24.3 ppm, respectively), allowing fast-tracking of molecular
evolution with ¹³C NMR. Therefore, each intermediate and
product were detected as two doublets because of ¹J_{CC} while
the nonlabeled positions remained invisible. To avoid any
possible influence of unreacted ACP on the mechanistic study,
¹³C-labelled ACP was added only in a slight excess.

In Step 1, the Claisen–Schmidt condensation was conducted under air at 80 °C (Figure 3A). The ACP

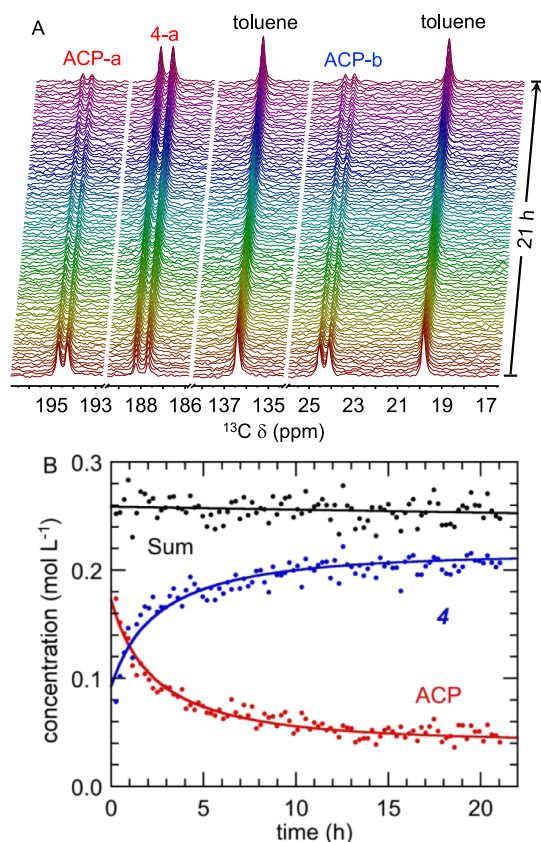


Figure 3. Claisen–Schmidt condensation reaction of ACP and NBA at 80 °C. (a) Arrays of direct polarization ^{13}C MAS-NMR spectra (MAS rate: 5 kHz, eight scans per transient); (b) kinetic analysis of time-resolved NMR spectra. The 5 mm NMR rotor was loaded with ACP- α,β - $^{13}\text{C}_2$ (1.56 mg, 12.8 μmol), and NBA (1.61 mg, 10.7 μmol) in 50 μL toluene with 1 wt % Pd/UiO-66 (1 mg). The curvefits (solid lines) were obtained by fitting the second-order rate equation.

resonances started to decrease in intensity with the appearance of two new doublets at 187.4 and 126.5 ppm (Figures 3A and S4), assigned to **4**. A trace amount of β -hydroxyketone intermediate **3** was detected when lowering the reaction temperature to 60 °C (Figure S5). No aldol product was observed between two ACP molecules at both tested temperatures. At 12 h, the yield of **4** was 80% based on ACP, and the selectivity was >99%; in addition, the total concentration stayed constant after 21 h. The concentration profiles of ACP and **4** were extracted from the NMR arrays acquired at 80 °C (Figure 3A). The time-resolved data of ACP and **4** were curve-fitted with second-order rate equations³⁵ (Figure 3B). The pseudo second-order rate constants of ACP and compound **4** were almost identical: 2.7 ± 0.1 and $2.6 \pm 0.2 \text{ M}^{-1} \text{ h}^{-1}$, respectively.

In Step 2, the rotor, further charged with 27.6 bar H_2 , was heated to 40 °C and maintained for 22 h. The high pressure of H_2 gas ensured a large excess of H_2 (ca. 15 \times of **4** by mol). Resonances of **4** disappeared after 2 h with the appearance of several sets of doublets (Figure 4). PTHQ (55.1 and 30.1 ppm) and PQ (155.7 and 117.2 ppm) were observed as the expected products. Two doublets at 195.7 and 37.9 ppm are assigned to the a and b carbons in **7**, arising from the reduction

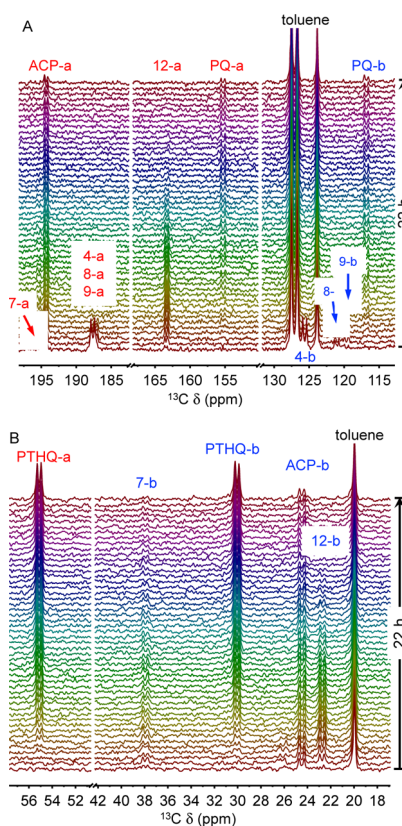


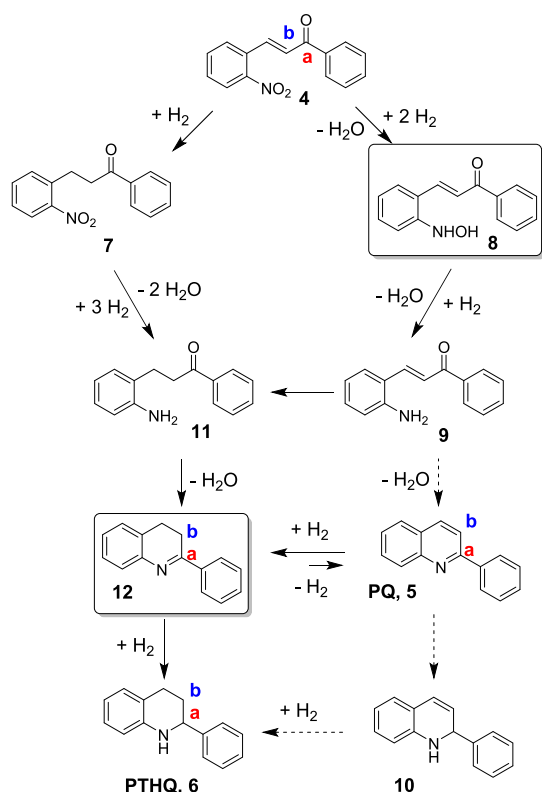
Figure 4. Arrays of direct polarization ^{13}C MAS-NMR spectra (eight scans per transient), recorded during reductive cyclization of **4** at 40 °C under 27.6 bar H_2 , showing (A) 198–113 and (B) 58–17 ppm. NMR rotor (5 mm), containing the reaction mixture after Claisen–Schmidt condensation, was pressurized with H_2 at 22 °C (MAS rate: 5 kHz).

of the $\text{C}=\text{C}$ in **4** (Scheme 3). The chemical shift of **7** is confirmed with an authentic sample of **7** (Supporting Information).

A new resonance at 121.4 ppm instantly appeared in the first spectrum and disappeared within 2 h, following which an adjacent signal at 120.0 ppm first formed and then disappeared. Pairing signals of these two new resonances (121.4 and 120.0 ppm) also partially overlap with **4**-a (187.6 ppm), indicating that the two new species preserve both $\text{C}=\text{O}$ and $\text{C}=\text{C}$ functionalities. The lower frequencies of the b carbons of these two new species are mostly because of the reduction of the $-\text{NO}_2$ group in **4**. Therefore, we can most likely assign the new peaks to **8** containing hydroxylamine and **9** with amine (Scheme 3). Compound **8** is an unstable molecule, and its *in situ* observation (up to 0.04 mol L^{-1}) is seldom reported. Few reports on the detection of phenylhydroxylamine are available with *in situ* and *ex situ* NMR but not under pressurized H_2 .^{36,37} The detections were only reported with *in situ* IR spectroscopy under pressure (10 bar H_2),^{38,39} but its quantification was not achieved. The formation of stable products and intermediates, PTHQ, PQ, **4**, **7**, and **9**, was also confirmed by *ex situ* HPLC–MS analysis of samples taken from a batch reactor after 30 min operating at 27.6 bar and 40 °C (Figure S6).

Compound **11**, the further hydrogenation intermediate from either **7** or **9**, cannot be identified in the NMR spectra, nor detected by either GC–MS or HPLC–MS. The absence of **11** is possibly because of its low concentration as it readily

Scheme 3. Reaction Networks of the Pd/UiO-66 Catalyzed Hydrogenation of 4 for the Synthesis of 6, as Demonstrated by the NMR Study^a



^aMolecules in solid box are unstable reaction intermediates. Solid lines represent transformations identified from experimental evidence. Dotted lines represent other possible transformations.

257 cyclizes. However, the detection of 7 can indirectly prove the
258 existence of 11 as a short-lived intermediate. The carbonyl
259 signals of 4, 7, 8, and 9 drift slightly to lower frequency, mostly
260 because of the interaction of their carbonyls with the side-
261 product water.

262 As shown in Figure 4, there is another set of two
263 pronounced doublets (163.7 and 22.7 ppm), which presum-
264 ably can be assigned to 2-phenyl-3,4-dihydroquinoline (12, in
265 Path III, Scheme 2), agreeing with the literature results.⁴⁰
266 Compound 12 cannot be detected by traditional chromato-
267 graphic techniques,⁴⁰ including thin layer chromatography
268 (TLC) (Figure S7), GC–MS, or HPLC–MS, most likely
269 because of its instability. Surprisingly, our operando NMR
270 result shows that the maximal concentration of compound 12
271 is as high as 0.11 mol L⁻¹ at 4 h. The direct identification of 12
272 was only once reported, but not quantified, during the direct
273 hydrogenation of quinones catalyzed by the homogeneous Ru
274 complex, using electro-spray ionization high-resolution mass
275 spectrometry.⁴⁰ This further demonstrates the unique capa-
276 bility of operando MAS-NMR in detection and quantification
277 of reactive intermediates to construct complex reaction
278 networks, while *ex situ* methods can only provide insufficient
279 or even misleading information.

280 Compound 12 can be formed either by an intramolecular
281 condensation reaction of 11 or partial reduction of PQ
282 (Scheme 3). The latter is rather unlikely under the reaction
283 condition because the maximal concentration of PQ, 0.02 mol
284 L⁻¹ (yield: 8%), was reached at 7 h, and further conversion of

PQ was not clearly observed (Figure S8). In addition, all
285 species before cyclization (4, 7, 8, and 9) were almost
286 consumed when 12 peaked, indicating that unobserved
287 compound 11 is the major source of 12 (Figure S8). The
288 concentration of PTHQ and 12 together with the sum of 4 + 7
289 + 8 + 9 are shown in Figure 5. The rate constant of 12
290 is

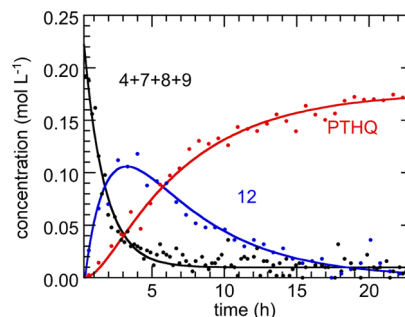


Figure 5. Concentration profiles of 12, PTHQ, and sum of 4, 7, 8, and 9, extracted from MAS-NMR arrays (Figure 4). For better presentation, only every third data point is shown for all curves except the sum of 4, 7, 8, and 9. Concentration profiles of PTHQ and 12 were analyzed with biexponential rate equations. Other line is added only to guide the eye.

consumption ($0.18 \pm 0.01 \text{ M}^{-1} \text{ h}^{-1}$) matches well with that of
291 PTHQ production ($0.16 \pm 0.01 \text{ M}^{-1} \text{ h}^{-1}$), obtained by
292 curvefitting according to a consecutive reaction kinetics with
293 two pseudo first-order reactions, which strongly suggests that
294 PTHQ is mostly derived from 12. The complete network of
295 reductive cyclization, based on operando NMR identified
296 intermediates, is thus shown in Scheme 3.
297

To better benchmark the relative rates of hydrogenation,
298 experiments starting with identified intermediate 7, in
299 comparison to 4 and PQ, were also conducted under two
300 conditions, 40 °C with 27.6 bar H₂ (Figure 6) and 50 °C with
301 66

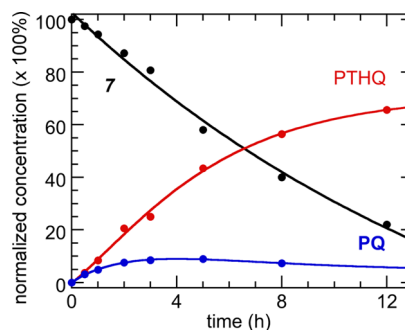


Figure 6. Time-resolved concentration profiles of the Pd/UiO-66-catalyzed hydrogenation reaction of 7 at 40 °C and 27.6 bar H₂. Reaction conditions: 7 (0.2 mmol), 2 wt % Pd/UiO-66 (5 mg, ~0.5 mmol % Pd), and solvent toluene (2 mL). Conversions were calculated based on analysis of GC results. Lines are added only to guide the eye.

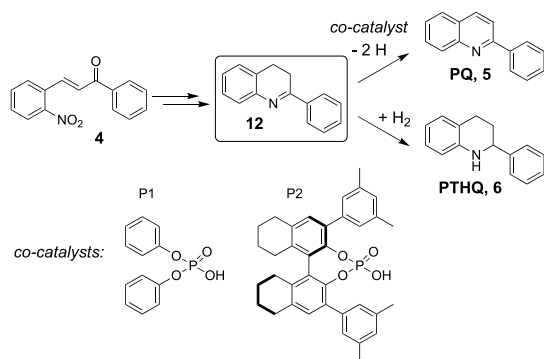
ambient H₂ (Figure S3). Under both conditions, the reaction
302 of 7 is slower than compound 4 but faster than PQ because 4
303 can be converted through two subsequent pathways (7 and 8)
304 (Scheme 3). The rate of PTHQ production from 4 and 7
305 (Figures 2A and 6) is almost identical. In addition, the
306 concentration build-up was clearly observed for 12 but not for
307 11. Together, these results suggest that the turnover-limiting
308 step is most likely the hydrogenation of 12. PQ cannot be
309

directly produced from **9** because **9** preserves the trans configuration of the corresponding starting material **4** with a large $^3J_{\text{HH}}$ coupling constant (15.5 Hz) of the olefinic protons. Therefore, PQ is yielded as a result of the Pd/UiO-66 catalyzed dehydrogenation of **12**. Similar dehydrogenation reactions have been reported as an equilibrium enabled by Pd-based catalysts for reversible hydrogen storage.⁴¹ The hydrogenation of **12** to PTHQ is faster than the dehydrogenation of **12** to PQ in the presence of H₂.

The mechanistic study clearly shows that Pd/UiO-66 can selectively favor the PTHQ formation pathway with a lower activation barrier, suggesting the advantage in using the reductive intramolecular cyclization reaction, when compared to the direct reduction of PQ. It should be noted that the full conversion of PQ to PTHQ via **12** can be achieved but under more forcing conditions (i.e., higher temperature).

Selective Production of PQ over PHTQ. The identification of reactive intermediates, that is **12**, allows us the ability of switching the product selectively from PTHQ to PQ by selectively enhancing the dehydrogenation of **12** to PQ. We employed two phosphoric acids as homogeneous transfer hydrogenation catalysts (Scheme 4), P1 with two phenyls and

Scheme 4. Hydrogenation of **4** with and without P1 and P2 Co-catalyst



P2 with an octahydro-BINOL derivative. P1 and P2 have been widely applied in transfer hydrogenation reactions with Hantzsch esters as the hydrogen sources.^{42,43} More importantly, both P1 and P2 are inert in H₂ activation,^{44–46} and phosphoric acids do not affect the structures and activity of Pd NPs for hydrogenation reactions,⁴⁷ particularly when accessibility of acid center in P2 is protected by the sterically restricting neighboring group.⁴⁸ Using the same reaction condition in the MAS-NMR study, all reactions initiating with **4** reached 100% conversion in 19 h with or without the use of co-catalysts (Table 1).

Without any co-catalyst, **4** converted to PTHQ in a high yield with only 1% of PQ (Table 1, entry 1); nevertheless, higher selectivity toward PQ (9%) was observed after adding 2 mol % P1 (Table 1, entry 2). Changing the co-catalyst to P2 (2 and 20 mol %) shifts the product selectivity more obviously, increasing the yield of PQ to 24 and 71%, respectively (Table 1, entries 3 and 4). It should be noted that the 71% yield of PQ was achieved under 27.6 bar H₂ in the presence of Pd. Furthermore, reactions starting with PTHQ did not yield PQ (Table 1, entries 5 and 6), suggesting PQ is solely generated from **12** in the presence of the co-catalyst. The success in the mechanism-inspired switch of the products on demand provides us an extra measure to achieve selective synthesis

Table 1. Hydrogenation of Different Substrates Catalyzed by Pd/UiO-66 with and without Co-catalysts^a

entry	substrates	co-catalyst	amount mol %	yield (%) ^b	
				PTHQ	PQ
1	4			95	1
2	4	P1	2	82	9
3	4	P2	2	70	24
4	4	P2	20	23	71
5	PTHQ				≤1
6	PTHQ	P2	20		≤1

^aReaction conditions: (1) **4** (0.1 mmol), 2 wt % Pd/UiO-66 (5 mg), toluene (1 mL), 40 °C, 27.6 bar H₂, and 19 h. ^bAll yields are calculated by GC with mesitylene as the internal standard.

which further demonstrates the importance of a molecular-level understanding of a reaction network in catalysis.

CONCLUSIONS

In conclusion, we have employed operando high-pressure MAS-NMR spectroscopy to construct the reaction network and achieve product selectivity in the synthesis of PTHQ and PQ. An acidic MOF-supported Pd NPs (Pd/UiO-66) as a bifunctional catalyst is used to achieve one-pot tandem synthesis. The acidic sites in UiO-66 were efficient in catalyzing the Claisen–Schmidt condensation between NBA and ACP, and the *in situ* formed *ortho*-nitrochalcone was reduced multistepwise by the supported Pd NPs under H₂, generating PTHQs in moderate to high isolated yields. Multiple stable and unstable intermediates were pinpointed and quantified under the operando condition, which allows the clear elucidation of the conversion pathways under 27.6 bar H₂. The mechanistic insights not only demonstrate a catalyst-enabled route for efficient chemical transformation under milder conditions but also allow us to selectively produce PQ or PTHQ via kinetic control of the conversion of the *in situ* observed key intermediate (**12**) employing a homogeneous co-catalyst in addition to heterogeneous Pd/UiO-66. The demonstrated methodology, that is, mechanistic study-guided design of catalytic systems, can be well applied to other tandem reactions with a complex reaction network involving multistep interconnected transformations of various functional groups.

ASSOCIATED CONTENT

Supporting Information

The Supporting Information is available free of charge at <https://pubs.acs.org/doi/10.1021/acscatal.0c00899>.

Examples for the synthesis of PTHQs and PQs, structural characterization of catalysts (physisorption and XRD), additional *ex situ* reactivity results, operando NMR and related analysis, and characterization of reaction species (PDF)

AUTHOR INFORMATION

Corresponding Authors

Long Qi – U.S. DOE Ames Laboratory, Iowa State University, Ames, Iowa 50010, United States; orcid.org/0000-0002-1213-2946; Email: lqi@iastate.edu
Zhiguo Zhang – Key Laboratory of Biomass Chemical Engineering of Ministry of Education, College of Chemical and Biological Engineering, Zhejiang University, Hangzhou 310027, 398

China; orcid.org/0000-0003-1681-4853;
Email: zhiguo.zhang@zju.edu.cn
Wenyu Huang – U.S. DOE Ames Laboratory and Department
of Chemistry, Iowa State University, Ames, Iowa 50010, United
States; orcid.org/0000-0003-2327-7259;
Email: whuang@iastate.edu

Authors

Jingwen Chen – Department of Chemistry, Iowa State
University, Ames, Iowa 50010, United States; Key Laboratory
of Biomass Chemical Engineering of Ministry of Education,
College of Chemical and Biological Engineering, Zhejiang
University, Hangzhou 310027, China
Biying Zhang – Department of Chemistry, Iowa State
University, Ames, Iowa 50010, United States
Renfeng Nie – Department of Chemistry, Iowa State University,
Ames, Iowa 50010, United States; orcid.org/0000-0002-4311-3465
Zhiyuan Qi – Department of Chemistry, Iowa State University,
Ames, Iowa 50010, United States
Takeshi Kobayashi – U.S. DOE Ames Laboratory, Iowa State
University, Ames, Iowa 50010, United States; orcid.org/0000-0002-6366-0925
Zongbi Bao – Key Laboratory of Biomass Chemical Engineering
of Ministry of Education, College of Chemical and Biological
Engineering, Zhejiang University, Hangzhou 310027, China;
orcid.org/0000-0003-4327-3028
Qiwei Yang – Key Laboratory of Biomass Chemical Engineering
of Ministry of Education, College of Chemical and Biological
Engineering, Zhejiang University, Hangzhou 310027, China;
orcid.org/0000-0002-6469-5126
Qilong Ren – Key Laboratory of Biomass Chemical Engineering
of Ministry of Education, College of Chemical and Biological
Engineering, Zhejiang University, Hangzhou 310027, China
Qi Sun – Key Laboratory of Biomass Chemical Engineering of
Ministry of Education, College of Chemical and Biological
Engineering, Zhejiang University, Hangzhou 310027, China

Complete contact information is available at:
<https://pubs.acs.org/10.1021/acscatal.0c00899>

Author Contributions

[†]L.Q. and J.C. are contributed equally.

Funding

J.C., Z.B., Q.Y., Q.R., and Z.Z. are grateful for financial support
from the National Key R&D Program of China
(2016YFA0202900), the National Natural Science Foundation
of China (21878266 and 21722609). J.C. thanks Zhejiang
University for financial support. We thank support from the
Iowa State University. L.Q. and T.K. are supported by the U.S.
Department of Energy (DOE), Office of Basic Energy
Sciences, Division of Chemical Sciences, Geosciences, and
Biosciences. The Ames Laboratory is operated for the U.S.
DOE by Iowa State University under Contract No. DE-AC02-
07CH11358. W.H. appreciate support from the National
Science Foundation (NSF) grant CHE-1566445.

Notes

The authors declare no competing financial interest.

ACKNOWLEDGMENTS

We thank Gordon J. Miller for the use of the XRD instrument.

ABBREVIATIONS

NMR, nuclear magnetic resonance; HPLC, high-performance
liquid chromatography; ESI–HRMS, electro-spray ionization
high-resolution mass spectrometry; TLC, thin layer chroma-
tography.

REFERENCES

- (1) Huang, Y.-B.; Liang, J.; Wang, X.-S.; Cao, R. Multifunctional
Metal–Organic Framework Catalysts: Synergistic Catalysis and
Tandem Reactions. *Chem. Soc. Rev.* **2017**, *46*, 126–157.
- (2) Li, X.; Zhang, B.; Tang, L.; Goh, T. W.; Qi, S.; Volkov, A.; Pei,
Y.; Qi, Z.; Tsung, C.-K.; Stanley, L.; Huang, W. Cooperative
Multifunctional Catalysts for Nitroene Synthesis: Platinum Nano-
clusters in Amine-Functionalized Metal–Organic Frameworks. *Angew.
Chem. Int. Ed.* **2017**, *56*, 16371–16375.
- (3) Hunger, M.; Weitkamp, J. In Situ IR, NMR, EPR, and UV/Vis
Spectroscopy: Tools for New Insight into the Mechanisms of
Heterogeneous Catalysis. *Angew. Chem. Int. Ed.* **2001**, *40*, 2954–2971.
- (4) Qi, L.; Alamillo, R.; Elliott, W. A.; Andersen, A.; Hoyt, D. W.;
Walter, E. D.; Han, K. S.; Washton, N. M.; Rioux, R. M.; Dumesic, J.
A.; Scott, S. L.; Walter, E.; Kee, H. S. Operando Solid-State NMR
Observation of Solvent-Mediated Adsorption-Reaction of Carbohy-
drates in Zeolites. *ACS Catal.* **2017**, *7*, 3489–3500.
- (5) Qi, L.; Chamas, A.; Jones, Z. R.; Walter, E. D.; Hoyt, D. W.;
Washton, N. M.; Scott, S. L. Unraveling the Dynamic Network in the
Reactions of an Alkyl Aryl Ether Catalyzed by Ni/ γ -Al₂O₃ in 2-
Propanol. *J. Am. Chem. Soc.* **2019**, *141*, 17370–17381.
- (6) Katritzky, A. R.; Rachwal, S.; Rachwal, B. Recent Progress in the
Synthesis of 1,2,3,4-Tetrahydroquinolines. *Tetrahedron* **1996**, *52*,
15031–15070.
- (7) Salas, P. F.; Herrmann, C.; Orvig, C. Metalloantimalarials. *Chem.
Rev.* **2013**, *113*, 3450–3492.
- (8) Wiesner, J.; Ortmann, R.; Jomaa, H.; Schlitzer, M. New
Antimalarial Drugs. *Angew. Chem. Int. Ed.* **2003**, *42*, 5274–5293.
- (9) Mukherjee, S.; Pal, M. Medicinal Chemistry of Quinolines as
Emerging Anti-Inflammatory Agents: An Overview. *Curr. Med. Chem.*
2013, *20*, 4386–4410.
- (10) Zemtsova, M. N.; Zimichev, A. V.; Trakhtenberg, P. L.;
Klimochkin, Y. N.; Leonova, M. V.; Balakhnin, S. M.; Bormotov, N. I.;
Serova, O. A.; Belanov, E. F. Synthesis and Antiviral Activity of
Several Quinoline Derivatives. *Pharm. Chem. J.* **2011**, *45*, 267.
- (11) Solomon, V. R.; Lee, H. Quinoline as a Privileged Scaffold in
Cancer Drug Discovery. *Curr. Med. Chem.* **2011**, *18*, 1488–1508.
- (12) Afzal, O.; Kumar, S.; Haider, M. R.; Ali, M. R.; Kumar, R.;
Jaggi, M.; Bawa, S. A Review on Anticancer Potential of Bioactive
Heterocycle Quinoline. *Eur. J. Med. Chem.* **2015**, *97*, 871–910.
- (13) Musiol, R. An Overview of Quinoline as a Privileged Scaffold in
Cancer Drug Discovery. *Expert Opin. Drug Discov.* **2017**, *12*, 583–597.
- (14) Crabtree, R. H. Hydrogen Storage in Liquid Organic
Heterocycles. *Energy Environ. Sci.* **2008**, *1*, 134–138.
- (15) Sridharan, V.; Suryavanshi, P. A.; Menéndez, J. C. Advances in
the Chemistry of Tetrahydroquinolines. *Chem. Rev.* **2011**, *111*, 7157–
7259.
- (16) Scott, J. D.; Williams, R. M. Chemistry and Biology of the
Tetrahydroisoquinoline Antitumor Antibiotics. *Chem. Rev.* **2002**, *102*,
1669–1730.
- (17) Hu, Z.; Zhao, D. Metal–Organic Frameworks with Lewis
Acidity: Synthesis, Characterization, and Catalytic Applications. *CrystEngComm*
2017, *19*, 4066–4081.
- (18) Hajek, J.; Vandichel, M.; Van de Voorde, B.; Bueken, B.; De
Vos, D.; Waroquier, M.; Van Speybroeck, V. Mechanistic Studies of
Aldol Condensations in UiO-66 and UiO-66-NH₂ Metal Organic
Frameworks. *J. Catal.* **2015**, *331*, 1–12.
- (19) Katz, M. J.; Mondloch, J. E.; Totten, R. K.; Park, J. K.; Nguyen,
S. T.; Farha, O. K.; Hupp, J. T. Simple and Compelling Biomimetic
Metal–Organic Framework Catalyst for the Degradation of Nerve
Agent Simulants. *Angew. Chem. Int. Ed.* **2014**, *53*, 497–501.

- (20) Granadeiro, C. M.; Ribeiro, S. O.; Karmaoui, M.; Valença, R.; Ribeiro, J. C.; De Castro, B.; Cunha-Silva, L.; Balula, S. S. Production of Ultra-Deep Sulfur-Free Diesels Using a Sustainable Catalytic System Based on UiO-66(Zr). *Chem. Commun.* **2015**, *51*, 13818–13821.
- (21) Yang, Q.; Xu, Q.; Jiang, H.-L. Metal-Organic Frameworks Meet Metal Nanoparticles: Synergistic Effect for Enhanced Catalysis. *Chem. Soc. Rev.* **2017**, *46*, 4774–4808.
- (22) Chen, L.; Luque, R.; Li, Y. Controllable Design of Tunable Nanostructures inside Metal-Organic Frameworks. *Chem. Soc. Rev.* **2017**, *46*, 4614–4630.
- (23) Rösler, C.; Fischer, R. A. Metal-Organic Frameworks as Hosts for Nanoparticles. *CrystEngComm* **2015**, *17*, 199–217.
- (24) Dhakshinamoorthy, A.; Garcia, H. Cascade Reactions Catalyzed by Metal Organic Frameworks. *ChemSusChem* **2014**, *7*, 2392–2410.
- (25) Jiang, J.; Yaghi, O. M. Brønsted Acidity in Metal–Organic Frameworks. *Chem. Rev.* **2015**, *115*, 6966–6997.
- (26) Hajek, J.; Caratelli, C.; Demuyne, R.; De Wispelaere, K.; Vanduyfhuys, L.; Waroquier, M.; Van Speybroeck, V. On the Intrinsic Dynamic Nature of the Rigid UiO-66 Metal–Organic Framework. *Chem. Sci.* **2018**, *9*, 2723–2732.
- (27) Hajek, J.; Bueken, B.; Waroquier, M.; De Vos, D.; Van Speybroeck, V. The Remarkable Amphoteric Nature of Defective UiO-66 in Catalytic Reactions. *ChemCatChem* **2017**, *9*, 2203–2210.
- (28) Pérez-Mayoral, E.; Jirí, Č. [Cu₃(BTC)₂]: A Metal–Organic Framework Catalyst for the Friedländer Reaction. *ChemCatChem* **2011**, *3*, 157–159.
- (29) Li, X.; Guo, Z.; Xiao, C.; Goh, T. W.; Tesfagaber, D.; Huang, W. Tandem Catalysis by Palladium Nanoclusters Encapsulated in Metal-Organic Frameworks. *ACS Catal.* **2014**, *4*, 3490–3497.
- (30) Davis, M. E.; Davis, R. J. *Fundamentals of Chemical Reaction Engineering*; Courier Corporation, 2012.
- (31) Dobereiner, G. E.; Nova, A.; Schley, N. D.; Hazari, N.; Miller, S. J.; Eisenstein, O.; Crabtree, R. H. Iridium-Catalyzed Hydrogenation of N-Heterocyclic Compounds under Mild Conditions by an Outer-Sphere Pathway. *J. Am. Chem. Soc.* **2011**, *133*, 7547–7562.
- (32) Erős, G.; Nagy, K.; Mehdi, H.; Pápai, I.; Nagy, P.; Király, P.; Tárkányi, G.; Soós, T. Catalytic Hydrogenation with Frustrated Lewis Pairs: Selectivity Achieved by Size-Exclusion Design of Lewis Acids. *Chem.—Eur. J.* **2012**, *18*, 574–585.
- (33) Walter, E. D.; Qi, L.; Chamas, A.; Mehta, H. S.; Sears, J. A.; Scott, S. L.; Hoyt, D. W. Operando MAS-NMR Reaction Studies at High Temperatures and Pressures. *J. Phys. Chem. C* **2018**, *122*, 8209–8215.
- (34) Chamas, A.; Qi, L.; Mehta, H. S.; Sears, J. A.; Scott, S. L.; Walter, E. D.; Hoyt, D. W. High Temperature/Pressure MAS-NMR for the Study of Dynamic Processes in Mixed Phase Systems. *Magn. Reson. Imag.* **2019**, *56*, 37–44.
- (35) Espenson, J. H. *Chemical Kinetics and Reaction Mechanisms*; McGraw-Hill: New York, 1995; Vol. 102.
- (36) Chen, G.; Xu, C.; Huang, X.; Ye, J.; Gu, L.; Li, G.; Tang, Z.; Wu, B.; Yang, H.; Zhao, Z.; Zhou, Z.; Fu, G.; Zheng, N. Interfacial Electronic Effects Control the Reaction Selectivity of Platinum Catalysts. *Nat. Mater.* **2016**, *15*, 564–569.
- (37) Gao, Y.; Ma, D.; Wang, C.; Guan, J.; Bao, X. Reduced Graphene Oxide as a Catalyst for Hydrogenation of Nitrobenzene at Room Temperature. *Chem. Commun.* **2011**, *47*, 2432–2434.
- (38) Richner, G.; van Bokhoven, J. A.; Neuhold, Y.-M.; Makosch, M.; Hungerbühler, K. In Situ Infrared Monitoring of the Solid/Liquid Catalyst Interface During the Three-Phase Hydrogenation of Nitrobenzene over Nanosized Au on TiO₂. *Phys. Chem. Chem. Phys.* **2011**, *13*, 12463–12471.
- (39) Corma, A.; Concepción, P.; Serna, P. A Different Reaction Pathway for the Reduction of Aromatic Nitro Compounds on Gold Catalysts. *Angew. Chem. Int. Ed.* **2007**, *46*, 7266–7269.
- (40) Wang, T.; Zhuo, L.-G.; Li, Z.; Chen, F.; Ding, Z.; He, Y.; Fan, Q.-H.; Xiang, J.; Yu, Z.-X.; Chan, A. S. C. Highly Enantioselective Hydrogenation of Quinolines Using Phosphine-Free Chiral Cationic Ruthenium Catalysts: Scope, Mechanism, and Origin of Enantioselectivity. *J. Am. Chem. Soc.* **2011**, *133*, 9878–9891.
- (41) Deraedt, C.; Ye, R.; Ralston, W. T.; Toste, F. D.; Somorjai, G. A. Dendrimer-Stabilized Metal Nanoparticles as Efficient Catalysts for Reversible Dehydrogenation/Hydrogenation of N-Heterocycles. *J. Am. Chem. Soc.* **2017**, *139*, 18084–18092.
- (42) Rueping, M.; Theissmann, T.; Antonchick, A. Metal-Free Brønsted Acid Catalyzed Transfer Hydrogenation-New Organocatalytic Reduction of Quinolines. *Synlett* **2006**, *2006*, 1071–1074.
- (43) Rueping, M.; Theissmann, T.; Raja, S.; Bats, J. W. Asymmetric Counterion Pair Catalysis: An Enantioselective Brønsted Acid-Catalyzed Protonation. *Adv. Synth. Catal.* **2008**, *350*, 1001–1006.
- (44) Fleischer, S.; Zhou, S.; Werkmeister, S.; Junge, K.; Beller, M. Cooperative Iron–Brønsted Acid Catalysis: Enantioselective Hydrogenation of Quinoxalines and 2 H-1,4-Benzoxazines. *Chem.—Eur. J.* **2013**, *19*, 4997–5003.
- (45) Qin, J.; Chen, F.; He, Y.-M.; Fan, Q.-H. Asymmetric Hydrogenation of 3-Substituted 2H-1,4-Benzoxazines with Chiral Cationic Ru-MsDPEN Catalysts: A Remarkable Counteranion Effect. *Org. Chem. Front.* **2014**, *1*, 952.
- (46) Chen, Q.-A.; Gao, K.; Duan, Y.; Ye, Z.-S.; Shi, L.; Yang, Y.; Zhou, Y.-G. Dihydrophenanthridine: A New and Easily Regenerable NAD(P)H Model for Biomimetic Asymmetric Hydrogenation. *J. Am. Chem. Soc.* **2012**, *134*, 2442–2448.
- (47) Chase, Z. A.; Fulton, J. L.; Camaioni, D. M.; Mei, D.; Balasubramanian, M.; Pham, V.-T.; Zhao, C.; Weber, R. S.; Wang, Y.; Lercher, J. A. State of Supported Pd During Catalysis in Water. *J. Phys. Chem. C* **2013**, *117*, 17603–17612.
- (48) Rueping, M.; Antonchick, A. P.; Theissmann, T. A Highly Enantioselective Brønsted Acid Catalyzed Cascade Reaction: Organocatalytic Transfer Hydrogenation of Quinolines and Their Application in the Synthesis of Alkaloids. *Angew. Chem. Int. Ed.* **2006**, *45*, 3683–3686.